CHINESE OPTICS LETTERS

Vol. 21, No. 10 | October 2023

Paper-based amorphous Ga_2O_3 solar-blind photodetector with improved flexibility and stability

Hanchi Xia (夏翰驰)[1], Tao Zhang (张 涛)[1], Yuehui Wang (王月晖)[1], Yaping Qi (祁亚平)[2,3], Fan Zhang (张 帆)[1*], Zhenping Wu (吴真平)[1**], and Yang Zhang (张 杨)[4***]

[1] State Key Laboratory of Information Photonics and Optical Communications & School of Science, Beijing University of Posts and Telecommunications, Beijing 100876, China

[2] Advanced Institute for Materials Research (WPI-AIMR), Tohoku University, Sendai 980-8577, Japan

[3] Department of Engineering Science, Faculty of Innovation Engineering, Macau University of Science and Technology, Macau 999078, China

[4] Institute of Modern Optics & Tianjin Key Laboratory of Micro-Scale Optical Information Science and Technology, Nankai University, Tianjin 300071, China

*Corresponding author: fzhang@bupt.edu.cn

**Corresponding author: zhenpingwu@bupt.edu.cn

***Corresponding author: yangzhang@nankai.edu.cn

Received April 13, 2023 | Accepted May 18, 2023 | Posted Online October 10, 2023

Flexible devices provide advantages such as conformability, portability, and low cost. Paper-based electronics offers a number of advantages for many applications. It is lightweight, inexpensive, and biodegradable, making it an ideal choice for disposable electronics. In this work, we propose a novel configuration of photodetectors using paper as flexible substrates and amorphous Ga_2O_3 as the active materials, respectively. The photoresponse characteristics are investigated systematically. A decent responsivity yield and a specific detectivity of up to 66 mA/W and 3×10^{12} Jones were obtained at a low operating voltage of 10 V. The experiments also demonstrate that neither the twisting nor bending deformation can bring obvious performance degradation to the device. This work presents a candidate strategy for the application of conventional paper substrates to low-cost flexible solar-blind photodetectors, showing the potential of being integrated with other materials to create interactive flexible circuits.

Keywords: amorphous Ga_2O_3; flexible photodetector; solar-blindness; paper.
DOI: 10.3788/COL202321.101601

1. Introduction

Flexible electronics is emerging as a new technology that can enable applications, including wearables, medical devices, solar cells, and displays. This technology offers solutions to many of today's challenges, such as energy efficiency and sustainability[1–4]. Photodetectors (PDs) have a wide range of uses in the fields of imaging, telecommunications, defense sensing, and ozone-hole monitoring as an essential branch of flexible optoelectronics. Due to their versatile properties, they are indispensable for a variety of cutting-edge applications. To develop wearable PDs, it is necessary to optimize key components such as substrates, electrodes, and light-absorption materials in order to fulfill the criteria of efficiency, light weight, flexibility, and stability[5–8]. Researchers have long focused on establishing wearable and flexible opto/electronic devices on nonbiodegradable polydimethylsiloxane (PDMS) and polyethylene terephthalate (PET) substrates in order to maximize their durability and performance[9–12]. On the other hand, the features of paper substrates such as light weight, easy availability, biodegradability, and nontoxicity make them a desirable choice for future intelligent electronics. With their cost-effectiveness and ability to produce ultralarge-area devices, paper provides an eco-friendly solution for commercial applications[13–16]. Recently, paper-based flexible ZnS/MoS_2 PDs have been proven to endure up to 10^2 to 10^3 of bending cycles without loss of stability, with a remarkable photoconductive responsivity of 17.8 μA/W[17]. WSe_2 nanodots have enabled the large-scale development of flexible PDs on paper substrates, and these have presented remarkable photoresponse abilities with a detectivity of 5.86×10^8 Jones, responsivity of 796.18 mA/W, and response time of 0.68 s[18].

Gallium oxide (Ga_2O_3) has grown increasingly popular in the past few decades due to its ultrawide bandgap semiconductor capabilities[19–25]. Its bandgap of around 4.9 eV fits nicely within the solar-blind spectrum of 200–280 nm, thus enabling PDs to detect light in this invisible ultraviolet (UV) range—unfathomable to the human eye[26–29]. These detectors can

facilitate clear imaging of an object even in direct sunlight, thus allowing for more precise sensing and monitoring. Solar-blind PDs are fundamental for a variety of applications, such as night vision, biological/chemical sensing, measuring air pollution, and detecting UV light. Ga_2O_3-based PDs are one kind of the intrigue semiconductors for solar-blind photodetection, providing use in devices for ozone hole detection and UV communication[26,30,31]. So far, flexible Ga_2O_3-based PDs are still rarely reported, which restricts their usability in more demanding environmental conditions such as wearable, flexible, and portable applications[7,32–34]. Herein, amorphous Ga_2O_3 (a-Ga_2O_3) thin films on ordinary printing-used paper were obtained by magnetron sputtering at room temperature. X-ray photoelectron spectroscopy (XPS) and UV-VIS absorbance spectrum measurements confirmed that the obtained Ga_2O_3 films had a stoichiometric ratio and a bandgap of 4.8 eV. Its solar-blind UV detection performance was tested through optical-coupled electrical measurements. The performance test results show that the paper-based film exhibits obvious solar-blind photoelectric response effect. Upon 254 nm illumination at 1000 $\mu W/cm^2$, the PDs exhibited an impressive responsivity of 66 mA/W, external quantum efficiency (EQE) of 20%, and photo-to-dark current ratio (PDCR) of 1×10^5. Further, to demonstrate the devices' compatibility under complicated deformation status when integrated on variant flexible electronic devices, we also conducted a flexing resilience test showing that the paper-based flexible PD retains good detectivity performance under and after various twisting angles and bending radii.

2. Experiments

High purity Ga_2O_3 ceramic (99.99%) with a 2-inch (1 inch = 2.54 cm) diameter was employed as the target (KJMTI Co., Ltd.), while commercial A4 paper was used as substrates. 500 nm thick a-Ga_2O_3 thin films were grown on the paper substrates through magnetron sputtering at room temperature with the following parameters: argon gas pressure of 0.5 Pa and sputtering power of 70 W. Au/Ti (30 nm/20 nm) interdigital electrodes were fabricated on the a-Ga_2O_3 film's surface using a hard mask and sputtering techniques. The schematic device structure diagram is shown in Fig. 1(a). X-ray diffraction (XRD) was utilized to study the amorphous nature of the as-grown films by means of a Bruker D8 Discover. XPS analysis was conducted via a Thermo ESCALAB 250xi. A Keithley 4200-SCS equipped with a probe station was used for photoresponse characteristics.

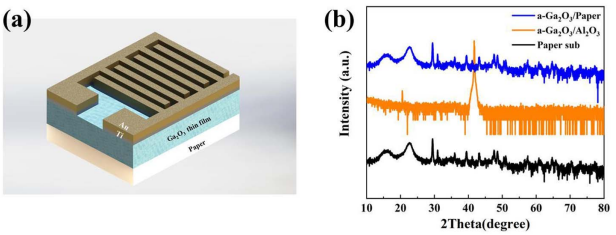

Fig. 1. (a) Schematic representation of the device; (b) XRD result for a-Ga_2O_3/paper sample; a-Ga_2O_3/Al_2O_3 and paper substrate XRD results are also displayed for comparison.

3. Results and Discussions

XRD measurements were carried out on the paper-based a-Ga_2O_3 film and compared to those obtained from sapphire substrates deposited at room temperature. As shown in Fig. 1(b), apart from the diffraction patterns from the paper substrates (mainly cellulose, along with other clay minerals, calcium carbonate, and titanium dioxide used for surface treatment), no diffraction peaks of the Ga_2O_3 film were detected. When the same deposition parameters were applied to the sapphire substrate, the film was still noncrystalline, with only the substrate signals detected in the XRD characterization. XPS is an analytical technique used to measure the binding energy of electrons emitted when the sample is bombarded with X rays, enabling it to identify the atomic composition, electronic structure, and chemical bonding state of the sample. All peak positions were calibrated using the C 1s peak at 284.8 eV. Figure 2(a) illustrates the survey for XPS spectra of deposited a-Ga_2O_3 thin film. The data are shown in the binding energy range of 0–1200 eV for the as-grown a-Ga_2O_3 film. No other elements peaks except for Ga, O, and C elements were observed within the sensitivity range of the technique in our sample. The Ga 2p spectrum [Fig. 2(b)] can be deconvoluted into two peaks with Ga $2p_{1/2}$ located at 1145.5 eV and Ga $2p_{3/2}$ located at 1118.5 eV. The separation energy value between these two peaks is about 27 eV, which is consistent with the binding energy (~26.9 eV) of the Ga 2p[35]. As shown in Fig. 2(c), the O 1s core level peak of a-Ga_2O_3 thin film is asymmetric; it can be divided into two components via the Gaussian fitting method, which is located at

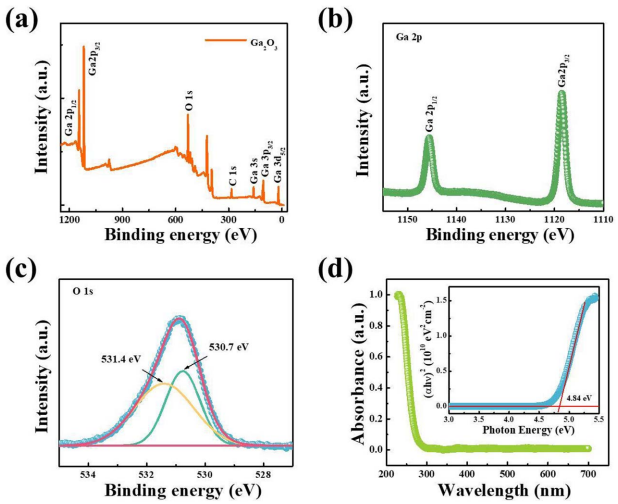

Fig. 2. (a) XPS survey spectrum of the as-grown a-Ga_2O_3 thin film; (b) core level of Ga 2p. (c) core level of O 1s; (d) UV-VIS absorbance spectrum of the a-Ga_2O_3 thin film with the plot of $(\alpha h\nu)^2$ versus $h\nu$ in the inset.

530.7 and 531.4 eV, respectively. The peak at 530.7 eV is assigned to lattice oxygen ions, and the peak at 531.4 eV is assigned to the oxygen ions in the oxygen vacancies region. The peak ratio of $I_{531.7}/(I_{530.4}+I_{531.7})$ is about 0.59, implying the existence of abundant oxygen vacancies in the film[36]. The oxygen vacancy in as-deposited a-Ga_2O_3 film can be attributed to the low temperature deposition process. As low substrate temperature (room temperature) has restricted the incorporation of oxygen into films, the as-deposited films have a great oxygen deficiency. To reveal the bandgap of a-Ga_2O_3, a UV-VIS absorbance spectrum is measured by comparing the intensity of light of different wavelengths that passes through the sample with the incident intensity for each wavelength. To obtain the absorbance spectrum, transparent substrates must be used for thin film deposition, with sapphire chosen for our experiment. Figure 2(d) shows a significant absorption edge at a wavelength of ~260 nm for the a-Ga_2O_3 thin film prepared on double-sided polished Al_2O_3 substrate under the same conditions as for the paper deposition. As a direct bandgap semiconductor, the bandgap of the a-Ga_2O_3 thin film is calculated by extrapolating the linear region of the plot of $(\alpha h\nu)^2$ versus $h\nu$ and taking the intercept on the $h\nu$ axis. The estimated bandgap is about 4.8 eV, as shown in the inset of Fig. 2(d), which is smaller than our previous results due to the oxygen deficiency.

Au/Ti interdigital electrodes are deposited using magnetron sputtering to form a metal–semiconductor–metal structure PD. The inset of Fig. 3(a) shows a picture of the fabricated device and also plots the dark current versus the voltage curve. This linear relationship between dark current and voltage confirms that an ohmic contact has been successfully obtained, as illustrated vividly. The dark current is approximately 23 pA at 10 V, which is extremely low. Figure 3(b) shows the *I*-*V* characteristics of the device under both dark and 254 nm light illumination, with a sequence of light intensities. The curves of current under different light intensities are differentiated by different colors. When the light intensity is below 100 μW/cm^2, a small increase in light intensity can cause a large increase in current. For example, compared to in dark and under 100 μW/cm^2 illumination, the current has an obvious improvement of up to 4 orders of magnitude. With the highest light intensity of 1500 μW/cm^2, the current under 10 V can reach 3×10^{-6} A. We have fitted the data from Fig. 3(b) to explore the relationship between current and light intensity, under 10 V bias. As illustrated in Fig. 3(c), the current increases with light intensity, showing that the device has good detectivity, even when light intensity is below 1 μW/cm^2. To further confirm the solar-blind band selectivity, the device's spectral response was studied. UV light with longer wavelengths corresponds to a lower excitation energy. As shown in Fig. 3(d), maximum responsivity is observed around 258 nm, which is consistent with the bandgap of a-Ga_2O_3 films (4.8 eV). This demonstrates that the prepared PDs have good spectral selectivity.

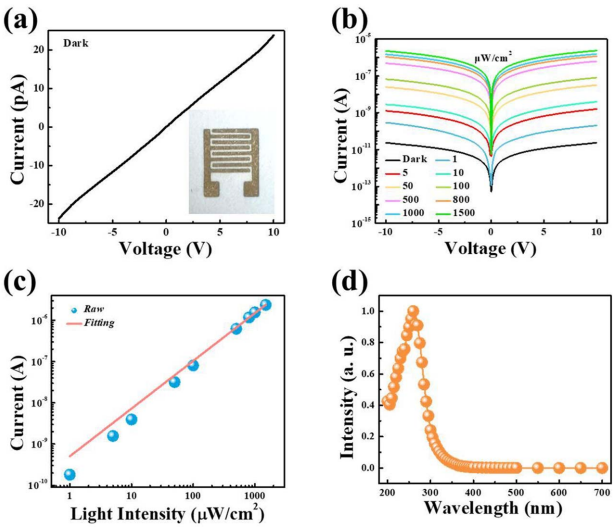

Fig. 3. (a) *I*-*V* characteristic of the Au/Ti-a-Ga_2O_3-Ti/Au structure, with inset showing the photograph of the flexible PDs; (b) *I*-*V* characteristic curves of the Ga_2O_3 PD in the dark and under 254 nm light illumination with various light intensities; (c) current as a function of the light intensity under a voltage bias of 10 V; (d) spectral response of PD.

The responsivity (R), detectivity (D^*), PDCR, and EQE are the four most important parameters used for the quantitative evaluation of detector performance[28]. These parameters were investigated under various light intensities at 10 V; the results are given in Fig. 4. R denotes the ratio of the photocurrent flowing in the PD to the incident optical power, which can be calculated using Eq. (1),

$$R=\frac{I_{\rm ph}-I_{\rm dark}}{P\cdot S}, \tag{1}$$

where $I_{\rm ph}$ and $I_{\rm dark}$ are photocurrent and dark current, P is light intensity, and S is the effective illumination area. In this work, R can reach a peak of 66 mA/W under 1000 μW/cm^2 254 nm illumination. The D^*, which indicates the capacity of the detector to detect the smallest signal, is calculated using Eq. (2),

$$D^*=\frac{RS^{\frac{1}{2}}}{(2eI_{\rm dark})^{\frac{1}{2}}}, \tag{2}$$

where R, S, and $I_{\rm dark}$ are given above, and e is the charge of the electron. The maximum D^* achieves 3×10^{12} Jones under 1000 μW/cm^2 254 nm illumination. PDCR is mathematically

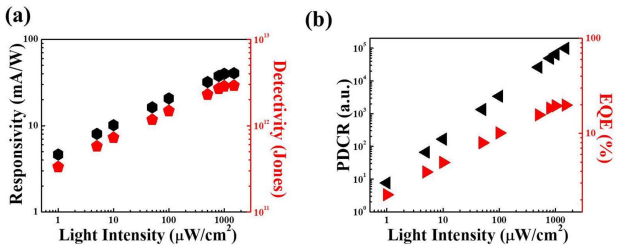

Fig. 4. (a) Responsivity and detectivity of the PDs at various light intensities; (a) PDCR and EQE of the PDs at various light intensities.

denoted as I_{ph}/I_{dark}, and is generally used to describe the anti-interference performance under background noise. From the figure it can be observed that the PDCR curve exhibits excellent linearity. The peak value can be attained to 1×10^5 under 1000 μW/cm^2 254 nm illumination. EQE, as a critical parameter for quantifying the behavior of PDs, can be evaluated from Eq. (3),

$$\mathrm{EQE}=\frac{I_{ph}}{P\cdot S}\times\frac{hc}{e\lambda}\times100\%, \tag{3}$$

where c is the speed of light, h is Planck's constant, e is the elementary charge, and λ is the wavelength of the incident light. As shown in Fig. 4(b), an EQE of 20% is achieved.

The excitation and migration of carriers takes time, meaning that the signal current from the PD does not reach the maximum value immediately upon incident light irradiation. The photocurrent of the device generally refers to the current after the incident light has stabilized. Usually, the faster the response speed of a PD, the better its performance is. The response speed of the PD can be quantified to evaluate the performance of the device response to transient irradiation generated by the power switching process. Usually, the rising edge τ_r and falling edge τ_d of the instantaneous current of the incident optical switch are used to characterize the response speed of the PD. In order to obtain the response speed of the detector, an exponential function fitting method was used to fit the change curve of the device's response current during the incident light irradiation switching on/off process. This enabled the estimation of the response times τ_r and τ_d, respectively,

$$I=I_0+A_1e^{\frac{-t}{\tau_1}}+A_2e^{\frac{-t}{\tau_2}}, \tag{4}$$

where I_0 is the photocurrent in steady state, A_1 and A_2 are constants, t is the time scale, and τ is the relaxation time constant. For our paper-based PD, the calculated response time values are shown in Fig. 5, where varying response speeds were achieved under different light intensities. Taking τ_{r1} and τ_{d1} as an identifiable signal, the response time of less than 1 s was achieved under different levels of illumination.

Flexible electronics generally requires devices to remain structurally intact and operational even after being subjected to twisting, bending, and stretching. For the paper-based devices, the stretching behaviors are always constrained by the mechanical properties of the paper used, which is generally unstretchable. Considering the actual working environment for the paper-based electronics, we conducted *I-V* measurements of the a-Ga_2O_3 flexible PD at various twisting angles under fixed illumination and bending radii. A twisting fixture was designed to twist the paper device at different angles. For the bending test, the paper device was attached to cylinders of different radii. In Figs. 6(a) and 6(b), it is shown that neither the twisting nor bending deformation had an obvious effect on performance. We did notice that in Fig. 6(b), there was a slight decrease in current when a smaller bending radius was applied. This could be attributed to the change in light illumination conditions, as

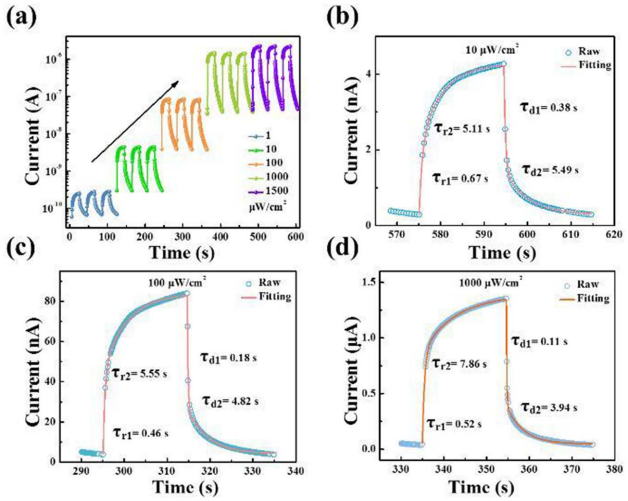

Fig. 5. (a) Temporal photoresponse of the detector at 10 V bias under 254 nm illuminations with different light intensities; response time of the device under 254 nm illuminations with (b) 10 μW/cm^2, (c) 100 μW/cm^2, and (d) 1000 μW/cm^2.

the light source we used was incident from a fixed position, and the bending changed the incidence angle. For devices being subjected to continuous mechanical disturbance, they should also be able to sustain their performance without any significant degradation after cycles of bending. In Figs. 6(c) and 6(d), the time-dependent photocurrent with different bendings applied and the intensity of the device's photocurrent as a function of the number of bending cycles at a bending radius of 8 mm were

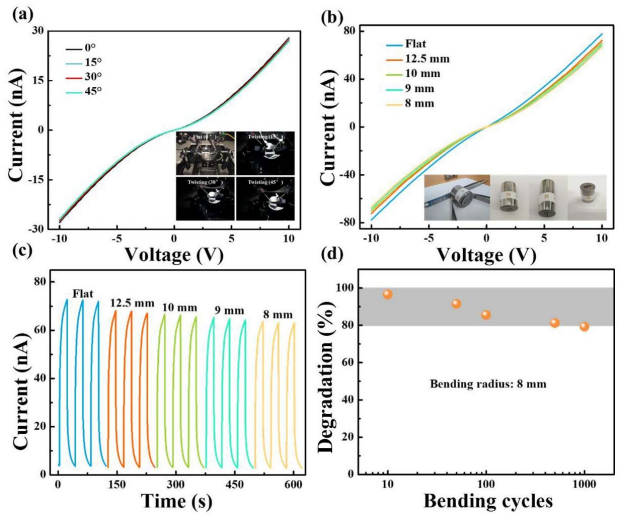

Fig. 6. (a) *I-V* characteristics of the a-Ga_2O_3 flexible PD with various twisting angles at fixed illumination; the inset is the digital image of the experimental setup. (b) *I-V* characteristics of the PD with different bending radii, with photographic image of the bending device before optoelectronic test in the inset; (c) time-dependence of the device for different bendings applied; (d) performance degradation of the photodetector as a function of the number of bending cycles at a bending radius of 8 mm.

measured. The results demonstrate good retention ability after 1000 cycles of bending.

4. Conclusion

In conclusion, we demonstrated a flexible solar-blind PD by depositing a-Ga_2O_3 on paper. Experimental results revealed that the a-Ga_2O_3 has a direct bandgap of 4.8 eV and shows good spectral selectivity within the solar-blind region. The responsivity, detectivity, PDCR, EQE, and response speed were characterized to verify the device performance of the paper-based PD. Furthermore, the flexible device was able to sustain its performance after cycles of mechanical disturbance. Our experiments showcase that the wide bandgap semiconductor Ga_2O_3 can be integrated into paper-based electronics, providing solutions to many of the challenges faced by flexible electronics.

Acknowledgement

This work was supported by the National Natural Science Foundation of China (Nos. 12274243, 11874230, 52233014, 51172208, and 12074044), the Fund of State Key Laboratory of Information Photonics and Optical Communications (No. IPOC2022ZT10), the Open Fund of IPOC (No. IPOC2022A02), and the Macau Science and Technology Development Fund (FDCT Grants 0106/2020/A3 and 0031/2021/ITP).

References

1. B. D. Gates, "Flexible electronics," Science **323**, 1566 (2009).
2. A. Nathan, A. Ahnood, M. T. Cole, S. Lee, Y. Suzuki, P. Hiralal, F. Bonaccorso, T. Hasan, L. Garcia-Gancedo, A. Dyadyusha, S. Haque, P. Andrew, S. Hofmann, J. Moultrie, D. Chu, A. J. Flewitt, A. C. Ferrari, M. J. Kelly, J. Robertson, G. A. J. Amaratunga, and W. I. Milne, "Flexible electronics: the next ubiquitous platform," Proc. IEEE **100**, 1486 (2012).
3. W. Gao, H. Ota, D. Kiriya, K. Takei, and A. Javey, "Flexible electronics toward wearable sensing," Acc. Chem. Res. **52**, 523 (2019).
4. Y.-C. Shen, C.-Y. Lee, H.-H. Wang, M.-H. Kao, P.-C. Hou, Y.-Y. Chen, W.-H. Huang, C.-H. Shen, and Y.-L. Chueh, "Embedded integration of Sb_2Se_3 film by low-temperature plasma-assisted chemical vapor reaction with polycrystalline Si transistor for high-performance flexible visible-to-near-infrared photodetector," ACS Nano **17**, 2019 (2023).
5. C. Xie and F. Yan, "Flexible photodetectors based on novel functional materials," Small **13**, 1701822 (2017).
6. W. Wu, X. Wang, X. Han, Z. Yang, G. Gao, Y. Zhang, J. Hu, Y. Tan, A. Pan, and C. Pan, "Flexible photodetector arrays based on patterned $CH_3NH_3PbI_{3-x}Cl_x$ perovskite film for real-time photosensing and imaging," Adv. Mater. **31**, 1805913 (2019).
7. Y. Wang, Z. Yang, H. Li, S. Li, Y. Zhi, Z. Yan, X. Huang, X. Wei, W. Tang, and Z. Wu, "Ultrasensitive flexible solar-blind photodetectors based on graphene/amorphous Ga_2O_3 van der Waals heterojunctions," ACS Appl. Mater. Interfaces **12**, 47714 (2020).
8. F. Liu, K. Liu, S. Rafique, Z. Xu, W. Niu, X. Li, Y. Wang, L. Deng, J. Wang, X. Yue, T. Li, J. Wang, P. Ayala, C. Cong, Y. Qin, A. Yu, N. Chi, and Y. Zhan, "Highly efficient and stable self-powered mixed tin-lead perovskite photodetector used in remote wearable health monitoring technology," Adv. Sci. **10**, 2205879 (2023).
9. Z. Lou and G. Shen, "Flexible photodetectors based on 1D inorganic nanostructures," Adv. Sci. **3**, 1500287 (2016).
10. Y. Zhang, P. Huang, J. Guo, R. Shi, W. Huang, Z. Shi, L. Wu, F. Zhang, L. Gao, C. Li, X. Zhang, J. Xu, and H. Zhang, "Graphdiyne-based flexible photodetectors with high responsivity and detectivity," Adv. Mater. **32**, 2001082 (2020).
11. T. Dong, J. Simões, and Z. Yang, "Flexible photodetector based on 2D materials: processing, architectures, and applications," Adv. Mater. Interfaces **7**, 1901657 (2020).
12. J. H. Mun, H. Lee, S. H. Lee, T.-S. Yoon, S. H. Han, and D. H. Kim, "Strain-induced photocurrent enhancement in photodetectors based on nanometer-thick ZnO films on flexible polydimethylsiloxane substrates," ACS Appl. Nano Mater. **3**, 10922 (2020).
13. D. B. Velusamy, J. K. El-Demellawi, A. M. El-Zohry, A. Giugni, S. Lopatin, M. N. Hedhili, A. E. Mansour, E. D. Fabrizio, O. F. Mohammed, and H. N. Alshareef, "MXenes for plasmonic photodetection," Adv. Mater. **31**, 1807658 (2019).
14. S. Cai, X. Xu, W. Yang, J. Chen, and X. Fang, "Materials and designs for wearable photodetectors," Adv. Mater. **31**, 1808138 (2019).
15. D. B. Velusamy, M. A. Haque, M. R. Parida, F. Zhang, T. Wu, O. F. Mohammed, and H. N. Alshareef, "2D organic-inorganic hybrid thin films for flexible UV-visible photodetectors," Adv. Funct. Mater. **27**, 1605554 (2017).
16. C. H. Lin, D. S. Tsai, T. C. Wei, D. H. Lien, J. J. Ke, C. H. Su, J. Y. Sun, Y. C. Liao, and J. H. He, "Highly deformable origami paper photodetector arrays," ACS Nano **11**, 10230 (2017).
17. P. T. Gomathi, P. Sahatiya, and S. Badhulika, "Large-area, flexible broadband photodetector based on ZnS–MoS_2 hybrid on paper substrate," Adv. Funct. Mater. **27**, 1701611 (2017).
18. P. Pataniya, C. K. Zankat, M. Tannarana, C. Sumesh, S. Narayan, G. Solanki, K. Patel, V. Pathak, and P. K. Jha, "Paper-based flexible photodetector functionalized by WSe_2 nanodots," ACS Appl. Nano Mater. **2**, 2758 (2019).
19. D. Guo, Q. Guo, Z. Chen, Z. Wu, P. Li, and W. Tang, "Review of Ga_2O_3-based optoelectronic devices," Mater. Today Phys. **11**, 100157 (2019).
20. S. J. Pearton, J. Yang, P. H. Cary, IV, F. Ren, J. Kim, M. J. Tadjer, and M. A. Mastro, "A review of Ga_2O_3 materials, processing, and devices," Appl. Phys. Rev. **5**, 011301 (2018).
21. Y. Yuan, W. Hao, W. Mu, Z. Wang, X. Chen, Q. Liu, G. Xu, C. Wang, H. Zhou, Y. Zou, X. Zhao, Z. Jia, J. Ye, J. Zhang, S. Long, X. Tao, R. Zhang, and Y. Hao, "Toward emerging gallium oxide semiconductors: a roadmap," Fundam. Res. **1**, 697 (2021).
22. Y. Wang, Y. Tang, H. Li, Z. Yang, Q. Zhang, Z. He, X. Huang, X. Wei, W. Tang, W. Huang, and Z. Wu, "p-GaSe/n-Ga_2O_3 van der Waals heterostructure photodetector at solar-blind wavelengths with ultrahigh responsivity and detectivity," ACS Photonics **8**, 2256 (2021).
23. J. Zhang, P. Dong, K. Dang, Y. Zhang, Q. Yan, H. Xiang, J. Su, Z. Liu, M. Si, J. Gao, M. Kong, H. Zhou, and Y. Hao, "Ultra-wide bandgap semiconductor Ga_2O_3 power diodes," Nat. Commun. **13**, 3900 (2022).
24. M. Higashiwaki, "β-Ga_2O_3 material properties, growth technologies, and devices: a review," AAPPS Bull. **32**, 3 (2022).
25. Y. Yang, H. Zhu, L. Wang, Y. Jiang, T. Wang, C. Liu, B. Li, W. Tang, Z. Wu, Z. Yang, and D. Li, "In-depth investigation of low-energy proton irradiation effect on the structural and photoresponse properties of ε-Ga_2O_3 thin films," Mater. Des. **221**, 110944 (2022).
26. D. Kaur and M. Kumar, "A strategic review on gallium oxide based deep-ultraviolet photodetectors: recent progress and future prospects," Adv. Opt. Mater. **9**, 2002160 (2021).
27. Q. Zhang, N. Li, T. Zhang, D. Dong, Y. Yang, Y. Wang, Z. Dong, J. Shen, T. Zhou, Y. Liang, W. Tang, Z. Wu, Y. Zhang, and J. Hao, "Enhanced gain and detectivity of unipolar barrier solar blind avalanche photodetector via lattice and band engineering," Nat. Commun. **14**, 418 (2023).
28. Y. Wang, H. Li, J. Cao, J. Shen, Q. Zhang, Y. Yang, Z. Dong, T. Zhou, Y. Zhang, W. Tang, and Z. Wu, "Ultrahigh gain solar blind avalanche photodetector using an amorphous Ga_2O_3-based heterojunction," ACS Nano **15**, 16654 (2021).
29. N. Li, Q. Zhang, Y. Yang, Y. Tang, T. Zhang, J. Shen, Y. Wang, F. Zhang, Y. Zhang, and Z. Wu, "Solar-blind avalanche photodetector based on epitaxial $Ga_2O_3/La_{0.8}Ca_{0.2}MnO_3$ pn heterojunction with ultrahigh gain," Chin. Opt. Lett. **21**, 051604 (2023).
30. Q. Cai, H. You, H. Guo, J. Wang, B. Liu, Z. Xie, D. Chen, H. Lu, Y. Zheng, and R. Zhang, "Progress on AlGaN-based solar-blind ultraviolet photodetectors and focal plane arrays," Light Sci. Appl. **10**, 94 (2021).

31. J. Chen, W. Ouyang, W. Yang, J.-H. He, and X. Fang, "Recent progress of heterojunction ultraviolet photodetectors: materials, integrations, and applications," Adv. Funct. Mater. **30**, 1909909 (2020).
32. S. J. Cui, Z. X. Mei, Y. H. Zhang, H. L. Liang, and X. L. Du, "Room-temperature fabricated amorphous Ga_2O_3 high-response-speed solar-blind photodetector on rigid and flexible substrates," Adv. Opt. Mater. **5**, 1700454 (2017).
33. Z. Li, Y. Xu, J. Q. Zhang, Y. L. Cheng, D. Z. Chen, Q. Feng, S. R. Xu, Y. C. Zhang, J. C. Zhang, Y. Hao, and C. F. Zhang, "Flexible solar-blind Ga_2O_3 ultraviolet photodetectors with high responsivity and photo-to-dark current ratio," IEEE Photon. J. **11**, 6803709 (2019).
34. J. Lai, M. N. Hasan, E. Swinnich, Z. Tang, S.-H. Shin, M. Kim, P. Zhang, and J.-H. Seo, "Flexible crystalline β-Ga_2O_3 solar-blind photodetectors," J. Mater. Chem. C **8**, 14732 (2020).
35. Q. Ren, W. Xu, Z. Shen, T. You, Q. Liu, C. Liu, L. Zhao, L. Chen, and W. Yu, "Solar-blind photodetector based on single crystal Ga_2O_3 film prepared by a unique ion-cutting process," ACS Appl. Electron. Mater. **3**, 451 (2021).
36. J. Yu, L. Dong, B. Peng, L. Yuan, Y. Huang, L. Zhang, Y. Zhang, and R. Jia, "Self-powered photodetectors based on β-Ga_2O_3/4H–SiC heterojunction with ultrahigh current on/off ratio and fast response," J. Alloys Compd. **821**, 153532 (2020).